

The diurnal variation of polarization characteristics of the Earth treated as an exoplanet

Shuang Wang^{1,2,3}, Zhong-Quan Qu^{1,3} and Hao Li^{1,3}

¹ Yunnan Observatories, Chinese Academy of Sciences, Kunming 650011, China; zqqu@ynao.ac.cn

² University of Chinese Academy of Sciences, Beijing 100049, China

³ Center for Astronomical Mega-Science, Chinese Academy of Sciences, Beijing 100101, China

Received 2018 August 13; accepted 2019 April 2

Abstract The diurnal polarization variation of the Earth, treated as an exoplanet with an unresolved disk but resolvable from its host star, is presented in three wavelength bands centered at 490 nm, 670 nm and 865 nm respectively according to French satellite-borne *PARASOL* data. We aim to estimate disk-integrated polarization of the Earth with a phase angle of 55° . It is shown that: (1) the linear polarization signal and its variation are ascribed to the combination of surface feature distribution and atmospheric conditions acting as a variable polarimetric modulator; and (2) the polarimetric wavelength dependence is strong due to the atmospheric wavelength sensitivity. During the period when the *PARASOL* data were acquired, the cloud coverage ranged from 44.0% to 57.7%, and the polarimetric diurnal variation amplitude was within 1.8% in the 490 nm band, 1.3% in the 670 nm band and 1.5% in the 865 nm band.

Key words: techniques: photometric — methods: data analysis — Earth

1 INTRODUCTION

Polarimetry has become a powerful method to characterize and detect exoplanets. For instance, the phase angle (the angle between the line-of-sight and the line connecting the star and planet) dependence of polarization characteristics of Mercury-like and Venus-like exoplanets was studied by Qu et al. (2013) and Batista & Stam (2014). Moreover, observations of Jupiter were performed by McLean et al. (2017) and theoretical calculations of Jupiter-sized exoplanets were acquired by Palmer et al. (2017). However, the most exciting thing is to search for those Earth-like exoplanets that have similar living condition as the Earth, such as an atmosphere with enough oxygen, a water ocean to support life, and so on. The main reason why polarimetry plays an important role in identifying atmosphere and surface features of exoplanets lies in the fact that the thickness of an atmosphere and different planetary surface features can induce evidently different polarization amplitudes and directions when the host star shines on it. In general, disk-integrated light irradiated from the host star can be considered to be unpolarized, while the starlight that is reflected by a planet will usually be polarized. The degrees of polarization depend on the planet's surface features and atmosphere. Recently, Ren & Serabyn (2006) and

Dou et al. (2015) made an effort to improve the technique to further the search for exoplanets, especially Earth-like exoplanets. As the constructions of large telescopes like the Thirty Meter Telescope (Atwood et al. 2014) and Giant Magellan Telescope (Szentgyorgyi et al. 2014) push ahead, and multi-conjugate adaptive optics (MCAO) are now applied for observations (Turri et al. 2015), a much higher spatial resolution will be achieved and thus the separation between the host star and planet will be observable for nearby exoplanets. This favors the ability to classify these exoplanets into different types.

A way to model terrestrial polarization is often examined in the literature. For example, Stam (2008) presented the fractional linear polarization from numerical simulations of Earth-like planets for wavelengths from 300 to 1000 nm at different phase angles. Stam modeled a planet at a phase angle of 50° with cloud coverage of 67.0% for a horizontally inhomogeneous planet at 440 nm and 870 nm, and obtained the diurnal variation as the planet rotates around its axis. The degree of polarization amplitude was calculated to be about 13.0%. No obvious diurnal variation was found at 440 nm but definite diurnal variation and periods were identified as shown in their figure 6. The degrees of polarization are around 1.0% from Stam's model at 870 nm. Karalidi & Stam (2012) reported numerical sim-

ulations of linearly polarized spectra from reflected light by clouds on exoplanets and found that they are sensitive to the clouds' parameters. Besides theoretical calculations of the Earth's polarization, studying Earth's polarimetric behaviors according to observational data has also emerged. Wolstencroft & Breon (2005) used POLDER to observe six main 'targets' of the Earth in three wavelength bands and different cloud coverages at a 90° phase angle. Utilizing earthshine is also a normal tool to estimate polarization properties of the Earth. Dollfus (1957) estimated polarization of the Earth from earthshine data. Sterzik et al. (2012) compared their observational results with a simulated signal of an Earth-like exoplanet based on POLDER data as well as simulations based on radiative transfer. They concluded that the degrees of polarization on 2011 April 25 are 9% and 4% larger than those observed from POLDER at 500 nm and 900 nm, respectively, at 90° phase angle, due to the lower cloud coverage. Moreover, their results are consistent with radiative transfer models in the blue spectral band, but much larger in the red band. Bazzon et al. (2013) measured earthshine polarization in the B , V , R and I bands for Earth at phase angles between 30° and 110° . They concluded that 65° is the best phase angle for detecting Earth-like exoplanets according to their calculations for four bands (see their fig. 14). In addition, their depolarization-corrected polarization signals at 55° phase angle in B , R and I bands are about 16.6%, 9.1% and 5.6%, respectively, according to their average over the mare and highland results.

French space-borne facility *Polarization and Anisotropy of Reflectances for Atmospheric Sciences coupled with Observations from a Lidar* (PARASOL) (<http://www.icare.univ-lille1.fr/>) is very suitable for the present study. We focus on the global polarization variation at the 55° phase angle. We obtain the global distributions of intensity I , fractional-linear polarizations Q/I and U/I with different cloud coverages of the Earth and then the disk-integrated polarimetric characteristics are calculated for daily variations in three wavelength bands centered at 490 nm, 670 nm and 865 nm, respectively. Finally, we compare our results with those from radiative transfer models and from earthshine.

Our purpose is to obtain Earth-like exoplanetary polarization signals by using PARASOL data and then to see how these results are consistent with radiative transfer models and observations from earthshine. We focus on a specific phase angle of 55° because we can obtain polarization data from almost the whole disk of Earth from PARASOL. This facilitates a comparison of our results with those of Stam (2008). Furthermore, this phase angle is near the rainbow phase angle region. Consequently, it would be helpful to understand the rainbow effect together with po-

larization signals at this phase angle. The polarization of Earth is determined by the atmosphere and surface properties, as well as various geometries. However, we cannot acquire sufficient data that contain enough geometries (various solar zenith angles, view zenith angles and relative azimuth angles) because PARASOL is a low orbit satellite. Nevertheless, the results we obtained from PARASOL could 'roughly estimate' the polarization properties of the Earth (Bailey 2007).

2 MODEL DESCRIPTIONS

For comparison purposes, we describe the planetary atmospheres and clouds modeled by Stam (2008). The model atmosphere contains 17 atmospheric levels, with total Rayleigh scattering optical thickness of 0.0975 at 550 nm, which is representative of an Earth-like exoplanetary atmosphere. Molecular absorbers such as ozone, oxygen and water are considered. Stam (2008) modeled spherical water-cloud droplets with a standard size distribution. The effective radius of the cloud droplets is $2.0 \mu\text{m}$ and the effective variance is $0.1 \mu\text{m}$. The refractive index of model cloud droplets is $1.33+0.0001i$, and cloud optical thickness is 10 at 550 nm, with the bottom of 802 hPa and top of 628 hPa.

3 DATA REDUCTION

Because of polarimetric imaging capability of a satellite-borne instrument, we adopt polarimetric data from French PARASOL. The instrument on PARASOL is similar to POLDER; however, the channel for longer polarized wavelengths was adopted at 490 nm instead of 443 nm on POLDER. Therefore linear polarimetry was carried out at three channels centered at 490 nm, 670 nm and 865 nm on PARASOL, and hereafter only those wavelengths will be referenced. PARASOL can acquire a sequence of images every 20 seconds, and the polarimetric instrument can record ground targets from different angles so that the Stokes parameters I , Q and U can be obtained. Here, we adopt the Anapol tool to analyze the PARASOL data. Anapol is an interface tool for POLDER and PARASOL data visualization and analysis (<http://www.icare.univ-lille1.fr/tools/Anapol>), and the polarization plane is finally defined with respect to the scattering plane according to the Anapol tool. However, because PARASOL's scientific goals are set for very local detection, the orbital heights are limited and then there are gaps between the spatially serial scanning strips, but we need a continuous mapping of the global polarization distribution by adopting data in the form of Level-1 products from PARASOL over two days (03/20/2006 and 03/21/2006). The surface of the Earth is divided into

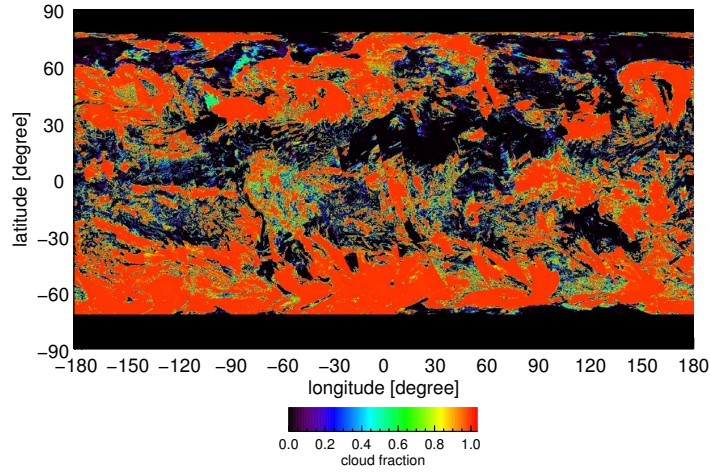


Fig. 1 Global cloud coverage distribution map.

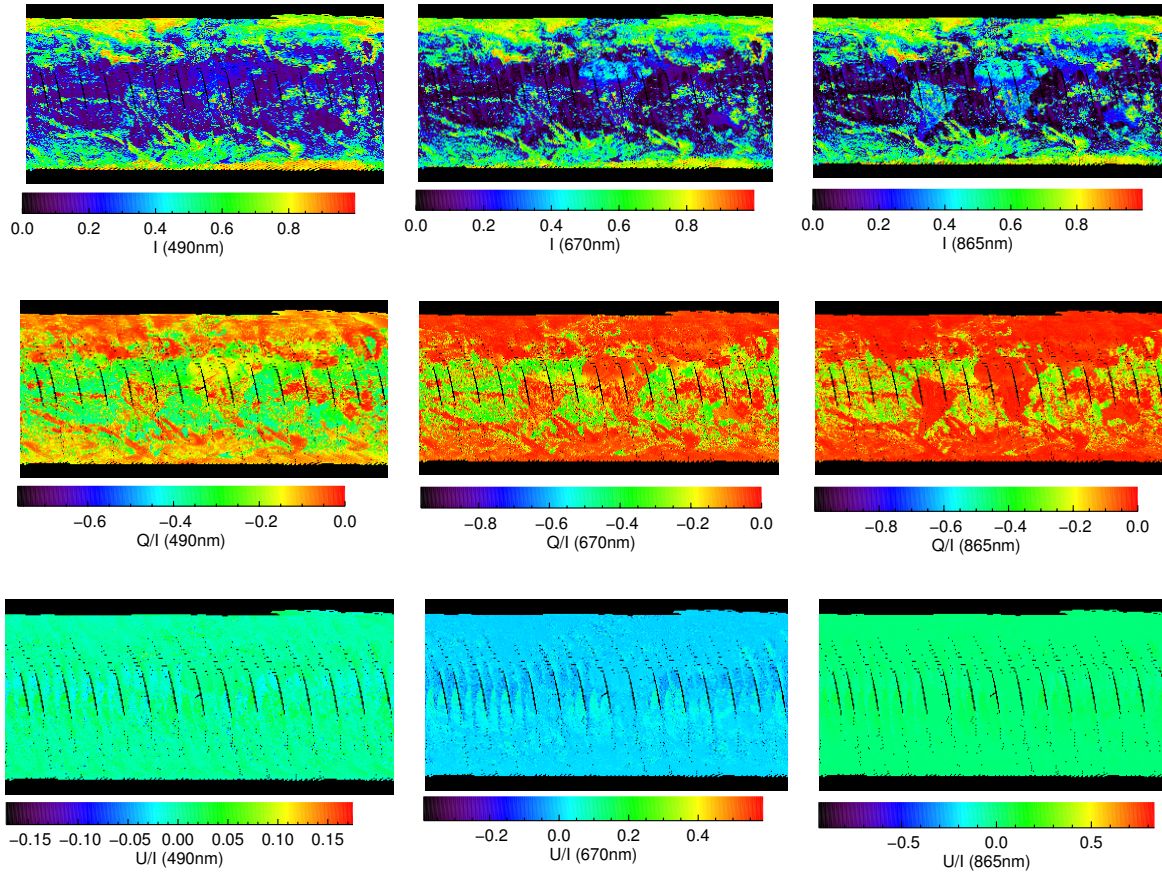


Fig. 2 I , Q/I and U/I maps at three wavelength bands. The top three panels present the intensity maps at 490 nm, 670 nm and 865 nm from left to right respectively. The middle three panels give Stokes Q/I maps at these three wavelength bands, and the bottom panels show the corresponding Stokes U/I maps. Note that the amplitudes of U/I are much smaller than those of Q/I .

360×180 Mercator grids. Because of a limitation associated with the orbit of *PARASOL*, we cannot acquire the global polarization data at arbitrary phase angles. However, we can get global polarization data at phase angle around 55° ($55^\circ \pm 1^\circ$). Thus $360 \times 180 = 64800$ samples are ex-

tracted globally from *PARASOL* data, and each of them should be representable for the polarimetric property of its local surface combined with the atmosphere. Stokes U/I values are close to 0 at all these wavelength bands. These reveal that the polarization directions are very near 90° .

Here the negative values of Stokes Q/I mean polarization perpendicular to the scattering plane. Thus the Q/I maps are close to degree of polarization maps. Furthermore, Stokes I parameter and polarization plane with respect to scattering plane can be produced with the Anapol tool. Thus the Stokes Q and U parameters can be obtained. The cloud map is derived from two days of *PARASOL* data (03/20/2006 and 03/21/2006). We divide the Earth's surface into a grid of $1^\circ \times 1^\circ$ units, which is much larger than the resolution of *PARASOL* ($6 \text{ km} \times 7 \text{ km}$ at nadir), thus we have to do spatial averaging. We generate a spatial average by averaging I , Q and U separately, and then compute the Q/I and U/I . After these operations, the global distributions of Stokes parameters I , Q/I and U/I , and cloud coverages can be plotted from Mercator projections. One can see that clouds are concentrated mainly in the high altitude regions, and they irregularly modulate the polarization (as will be seen later). The black longitudinal lines represent the gaps in *PARASOL* observations. Because they cover very small areas, these gaps do not significantly influence the polarimetric results.

Because the data used were acquired around vernal equinox, sunlight is assumed to be perpendicularly incident on the equator. This assumption simplifies the calculation. The geometry of longitude 0° is accepted as the starting longitude (see the top-left map of Fig. 3), and the other geometries are defined corresponding to the Earth's rotation. The longitude span covers 125° in each case.

4 RESULTS

In this section, we first present the global map of cloud coverage, and I , Q/I and U/I parameters. Then results of the diurnal variations of disk-integrated polarimetric characteristics are provided.

4.1 Global Distributions of Stokes Parameters and Cloud Fractions

There is a strong correlation in the cloud coverage map (Fig. 1) with reflectance maps at these wavelengths (see the top panels of Fig. 2). This is not strange because the existence of clouds usually means a higher reflectance. However, some difference between the reflectance map in the 490 nm band and corresponding maps in the other two bands is easily visible, especially in the middle of the map where South America is located. There is more reflectance when the wavelength is longer. This mainly happens because more light is reflected by the surface at longer wavelengths, since Rayleigh scattering is significantly reduced at longer wavelengths. In more detail, Rayleigh scattering produces the highest, 100% polarization, thus it is very important. However, the efficiency of Rayleigh scattering dra-

matically decreases as wavelength increases, thus Rayleigh scattering contributes much less to the total polarization at longer wavelengths and this decreases the total polarization. For Stokes Q/I , the continents become more visible at longer wavelengths because the atmosphere plays a less important role as the wavelength increases. The polarization values are mainly located between 0% and 40% at 490 nm, and between 0% and 30% at the two other wavelength bands. It can clearly be seen that the high latitudes generally correspond to lower degrees of polarization, which are mainly due to cloud coverage and surfaces.

4.2 Disk-integrated Polarization of the Earth

After giving the global polarization distributions of the Earth, we then integrate the polarization signals of the Earth's disk. To fill in the gaps in the low latitude areas, we apply suitable interpolations. The disk-integrated polarization signals at three wavelength bands (centered at 490 nm, 670 nm and 865 nm) are obtained according to equation (2) of Karalidi & Stam (2012). In more detail, we calculate the total I , Q and U , respectively, and then the disk-integrated polarization can be calculated. Our disk-integrated method is a weighted-sum method, just as used by Wolstencroft & Breon (2005). We adopt a method presented by Bailey (2007) to get the planetary polarization signals from *PARASOL* data.

We collect 36 snapshots in steps of 10° during a rotation period. As pointed out previously, because of the observational limitation of *PARASOL* due to its orbits, we fail to acquire polarization data on the polar regions (latitude higher than 78° near the North Pole and -72° near the South Pole). For the disk-integrated polarization with contributions from the polar regions, we fill polarization data from the polar regions by those of their neighboring pixels. Given that the viewing geometry varies strongly at the poles, it may strongly influence the disk-integrated polarization. Our estimating errors from the edge areas and glint areas are plotted in Figure 4.

4.3 Disk-integrated Polarization with Rotation of the Earth

Given the orbital limitation of *PARASOL*, we choose the phase angle at 55° . The data were obtained on 2006 March 20 and 2006 March 21, when the Sun passed over the equator, and thus the scattering plane coincided with the equatorial plane.

It is hard to determine the polarization of the edge regions and glint areas of a genuine Earth-like planet. Therefore, we will now estimate how much error will arise from the edge regions and glint areas. First, we set the degrees of polarization at edge regions and glint areas as 0%

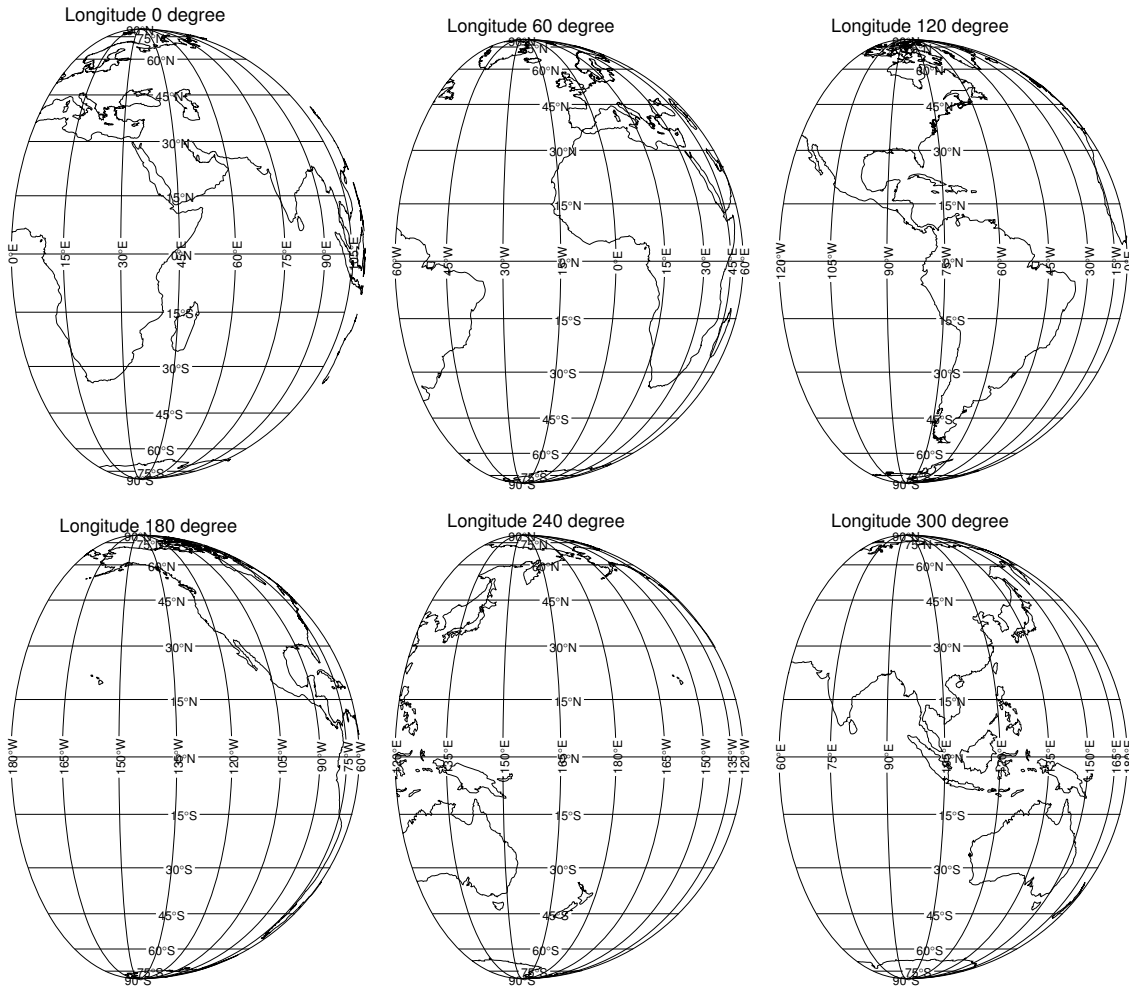


Fig. 3 Different fields of view for longitude as the Earth rotates.

Table 1 Disk-integrated Polarization Signals with Cloud occupation Fraction at *PARASOL* Polarimetric Bands

Starting longitude	Cloud fraction	P (490 nm)	P (670 nm)	P (865 nm)
10°	45.5%	12.23%	6.01%	3.83%
200°	55.2%	13.13%	7.33%	5.26%
220°	57.7%	12.71%	7.12%	5.17%

The second row shows the minimum in degrees of polarization at 670 nm and 865 nm. The third row gives the maximum in degrees of polarization at 490 nm and 670 nm. The bottom row presents the maximum cloud fraction and the corresponding polarization signals.

to estimate the minimum polarization. Afterwards, the degrees of polarization at those areas are then set as their maximum values (43% for 490 nm, 57% for 670 nm and 56% for 865 nm). In this way we can roughly obtain the error bars of the disk-integrated degrees of polarization. The edge regions occupy 3° of longitude. Moreover, the glint occurs at a specular reflective area, and the glint area is from 57° to 68° longitudinal distance with respect to the left edge longitude. As we can see from Figure 4, this assumption may introduce some errors while estimating the disk-integrated polarization through *PARASOL* data. We

can see clearly the diurnal polarimetric variation when different cloud coverages are applied, and the surface characteristics come in and then go out of the field of view. In particular, the maximum disk-integrated polarization amplitudes reach 13.13%, 7.33% and 5.29% at 490 nm, 670 nm and 865 nm respectively, while the minimum degrees of polarization are 11.36%, 6.01% and 3.83%, respectively. The variation amplitude is less than 2%. Degrees of polarization show a strong dependence on wavelength. The shorter the wavelength is, the greater the resulting polarization.

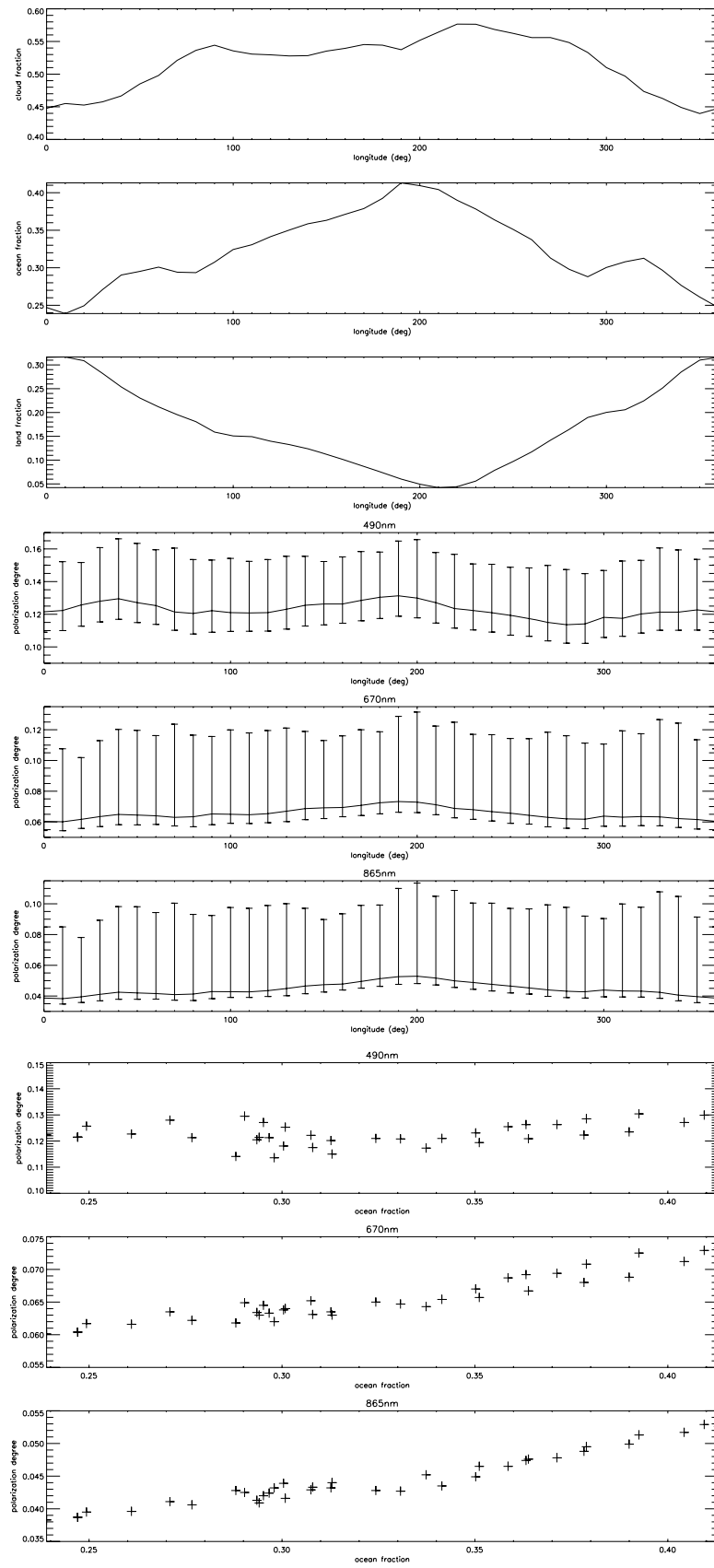


Fig. 4 Cloud, ocean and land distributions (*upper panels*), variations in degree of polarization during rotation of the Earth (*middle panels*) and polarization versus ocean fraction (*bottom panels*).

This contribution is calculated by filling in the grids by their neighboring regions along the same longitude, because the surface features are the same. It is easily seen from Table 1 that no visible variation can be found because both the area occupied and polarization due to snow are very small.

The top of Figure 4 plots the cloud fraction curve that is derived from *PARASOL* and the polarization variation curves for these bands. The variations in polarization are only more pronounced at 490 nm because polarization is stronger at 490 nm. In detail, during one day, the two variation periods happen for the 490 nm band. For the other two bands, it seems that only one period takes place. As pointed out earlier, the difference also lies in the polarization amplitudes. Now, we focus on the degree of polarization at 220° longitude as a starting longitude where the cloud fraction reaches its maximum. The degrees of polarization for these three bands do not reach their minimum, for instance the minimum polarization of 670 nm is 6.01%, but it occurs at 10° longitude. As clearly shown in Figure 4, there is no obvious relation between polarization and ocean fraction at 490 nm, but the polarization increases with an increasing ocean fraction at 670 nm and 865 nm. This demonstrates that not only the clouds but also surface features such as oceans can contribute significantly to the disk-integrated polarization if a thick cloud does not cover all of the Earth's surface features.

Generally speaking, the degree of polarization will increase as the cloud coverage decreases because multiple scatterings in the clouds provide a small contribution to the polarization, while most surface features are more productive in generating polarization such as ocean and forests. This can be easily ascertained in Figure 4. For instance, the largest cloud fraction occurs at starting longitude 220° and the degrees of polarization in these bands are relatively low. However, the maximum cloud fraction does not result in the minimum degree of polarization. As listed in Table 1, the maximum cloud fraction reads as 57.7% at starting longitude 220° and the corresponding degree of polarization is 5.17% at 865 nm, which is larger than its polarization minimum of 3.83% at longitude 10° . This may be caused by the different distributions of the clouds. For example, Karalidi & Stam (2012) conclude that the degree of polarization of Earth depends not only on cloud coverage but also on its locations. Otherwise, while the Earth spins, the atmosphere and apparent surfaces are also changed. However, the coverage of landscapes and oceans changes periodically but the cloud distribution does not show such a period at one phase angle. The polarimetric results originate from the combination of surfaces and clouds, while the latter plays a role of modulations.

To verify these findings, we compare our results with theoretical calculations and observational results from earthshine. Stam modeled a planet at a phase angle of 50° with 67.0% cloud coverage over a horizontally inhomogeneous planet at 440 nm and 870 nm (Stam 2008). The surface model of the planet was covered by oceans and vegetation. The degree of polarization was calculated to be about 13.0%, which is close to our result. However, at 490 nm, no obvious diurnal variation was found at 440 nm by them but definite diurnal variation and periods are found as shown in their figure 6. The degrees of polarization are around 1.0% from Stam's model at 870 nm, while our results are slightly larger (see their fig. 6 diurnal variation at 865 nm). This difference can be ascribed to our lower cloud coverage and larger phase angle that we adopted. The consistency between our results and those of Stam may indicate that the cloud properties are similar to those adopted by Stam (2008) as described in Section 2.

Karalidi & Stam (2012) modeled an Earth-like exoplanet with a black ocean and a central sandy continent. The Rayleigh scattering optical thickness is 0.1 at 550 nm, the cloud particles are described by a standard distribution with an effective radius of $2.0 \mu\text{m}$ and an effective variance of $0.1 \mu\text{m}$, and the cloud optical thickness is 2, smaller than that in Stam (2008). A comparison with conclusions from Karalidi & Stam (2012) reveals that their degree of polarization is about 16.0% at phase angle 55° with 42.3% cloud coverage using the HI-code, meanwhile, our result is 13.13% at 490 nm with a cloud coverage of 55.2% (see Table 1, longitude 200° as starting longitude), which is less than their result due to the smaller cloud optical thickness they use and a larger cloud fraction in our case. However, our results are smaller than theirs, although the cloud coverage is close to theirs. For instance, our result is 12.23% at 490 nm with a cloud coverage of 45.5% (see Table 1, 10° as starting longitude). This may be interpreted as smaller cloud optical thickness they used than Stam (2008), since our results are consistent with those of Stam (2008).

Finally, let us make a comparison with the observational results from earthshine. Bazzon et al. (2013) measured the earthshine polarization signals at various phases in *B*, *V*, *R* and *I* bands. They demonstrate that there are depolarization differences between mare and highlands. Their depolarization-corrected polarization signals at 55° phase angle in *B*, *R* and *I* bands are about 16.6%, 9.1% and 5.6% respectively according to their average results over the mare and highlands. Our results (13.13%, 7.33% and 5.26% at 490 nm, 670 nm and 865 nm respectively) are slightly less than their observational results. The good agreement between our weighted mean polarization results and those from Bazzon et al. (2013) may confirm our work's validity.

5 SUMMARY AND DISCUSSION

Generally speaking, polarization signals of the Earth are determined by atmosphere and surface properties, as well as geometries (solar zenith angles, viewing zenith angles and relative azimuth angles). However, various geometries cannot be obtained by *PARASOL* because of its low orbit. Consequently, we ‘roughly estimate’ the polarization properties of the Earth, and these results may help to characterize an Earth-like exoplanet in the future.

In this paper, we present the diurnal global polarization signals in three wavelength bands as the Earth is treated as a planet with an unresolved disk but resolved from the host star in the backward scattering (phase angle 55°) direction. We calculate the linear polarization and its diurnal variation, and find the following features:

1. The maximum disk-integrated polarization amplitudes reach 13.13%, 7.33% and 5.29% at 490 nm, 670 nm and 865 nm respectively, while the minimum degrees of polarization are 11.36%, 6.01% and 3.83% respectively.

2. The variation amplitude is less than 2% in a diurnal spin period.

3. The polarization magnitudes show a strong dependence on wavelength. The shorter the wavelength is, the greater the polarization becomes. This happens because the atmosphere plays a less important role as the wavelength increases and also because the contribution of Rayleigh scattering to the total intensity decreases at longer wavelengths. The decrease of polarization with wavelength and its fraction may indicate specific cloud composition and particle size.

Besides cloud coverage, we find that the ocean fraction will also influence polarization, because the polarization increases with increasing ocean fraction at 670 nm and 865 nm (as depicted in Fig. 4). This demonstrates an important property in that the diurnal polarization signals depend strongly on the distribution of cloud and surface features.

Acknowledgements We are grateful to the ICARE Data Release and Services Center for providing access to the data used in this study (<http://www.icare.univ-lille1.fr/>). This work is sponsored by the National Natural Science Foundation of China (NSFC) (Grant Nos. 11527804, 10943002 and 11373023). We are thankful for the comments of the reviews.

References

- Atwood, J., Skidmore, W., Anupama, G. C., et al. 2014, in Proc. SPIE, 9150, Modeling, Systems Engineering, and Project Management for Astronomy VI, 915013
- Bailey, J. 2007, *Astrobiology*, 7, 320
- Batista, S. F. A., & Stam, D. M. 2014, European Planetary Science Congress, 9, EPSC2014
- Bazzon, A., Schmid, H. M., & Gisler, D. 2013, *A&A*, 556, A117
- Dollfus, A. 1957, *Supplements aux Annales d’Astrophysique*, 4, 3
- Dou, J., Ren, D., & Zhu, Y. 2015, IAU General Assembly, 22, 2255996
- Karalidi, T., & Stam, D. M. 2012, *A&A*, 546, A56
- McLean, W., Stam, D. M., Bagnulo, S., et al. 2017, *A&A*, 601, A142
- Palmer, C., Stam, D., & Rossi, L. 2017, European Planetary Science Congress, 11, EPSC2017
- Qu, Z. Q., Sun, J., Song, W., & Yan, X. L. 2013, *Planet. Space Sci.*, 78, 33
- Ren, D., & Serabyn, E. 2006, in Proc. SPIE, 6265, 62653X
- Stam, D. M. 2008, *A&A*, 482, 989
- Sterzik, M. F., Bagnulo, S., & Palle, E. 2012, *Nature*, 483, 64
- Szentgyorgyi, A., Barnes, S., Bean, J., et al. 2014, in Proc. SPIE, 9147, Ground-based and Airborne Instrumentation for Astronomy V, 914726
- Turri, P., McConnachie, A. W., Stetson, P. B., et al. 2015, *ApJ*, 811, L15
- Wolstencroft, R. D., & Breon, F.-M. 2005, in *Astronomical Society of the Pacific Conference Series*, 343, *Astronomical Polarimetry: Current Status and Future Directions*, eds. A. Adamson, C. Aspin, C. Davis, & T. Fujiyoshi, 211